

## Analysis of the instability growth rate during the jet–background interaction in a magnetic field

Miroslav Horký<sup>1,2</sup> and Petr Kulhánek<sup>1</sup>

<sup>1</sup> Czech Technical University in Prague, Faculty of Electrical Engineering, Department of Physics, Technická 2, 166 27 Prague, Czech Republic; [horkymi1@fel.cvut.cz](mailto:horkymi1@fel.cvut.cz)

<sup>2</sup> Astronomical Institute of the Academy of Sciences of the Czech Republic, Boční II 1401/1a, 141 31 Prague 4, Czech Republic

Received 2012 October 31; accepted 2013 February 13

**Abstract** The two-stream instability is common, responsible for many observed phenomena in nature, especially the interaction of jets of various origins with the background plasma (e.g. extragalactic jet interacting with the cosmic background). The dispersion relation that does not consider magnetic fields is described by the well-known Buneman relation. In 2011, Bohata, Břeň and Kulhánek derived the relation for the two-stream instability without the cold limit, with the general orientation of a magnetic field, and arbitrary stream directions. The maximum value of the imaginary part of the individual dispersion branches  $\omega_n(k)$  is of interest from a physical point of view. It represents the instability growth rate which is responsible for the onset of turbulence mode and subsequent reconnection on the scale of the ion radius accompanied by a strong plasma thermalization. The paper presented here is focused on the non-relativistic instability growth rate and its dependence on various input parameters, such as magnitude and direction of magnetic field, sound velocity, plasma frequency of the jet and direction of the wave vector during the jet – intergalactic medium interaction. The results are presented in plots and can be used for determination of the plasma parameter values close to which the strong energy transfer and thermalization between the jet and the background plasma occur.

**Key words:** plasmas — methods: numerical — instabilities — turbulence — waves — MHD

### 1 INTRODUCTION

The most common plasma instabilities are the two-stream instabilities, which can occur during a plasma jet interaction with the plasma background. Such situations are observed in astrophysical processes, e.g. interaction of galactic jets with the intergalactic medium (e.g. Silk et al. 2012, and references therein) or interaction of star jets with the interstellar medium (Murphy et al. 2008). Oscar Buneman derived the basic dispersion relation describing such instabilities in the late 1950s for cold unmagnetized plasmas (Buneman 1959). The magnetohydrodynamic instabilities in an ideal plasma are discussed in Bonanno & Urpin (2011). Magnetic fields are crucial for the phenomena taking place in jets (Urpin 2006). In 2011, Bohata et al. published a paper containing the derivation of the non-relativistic dispersion relation for magnetized plasmas without the cold limit restriction (Bohata

et al. 2012). It is called the Generalized Buneman Dispersion Relation (GBDR) and is described by the equation

$$\prod_{\alpha=1}^2 \left\{ \Omega_{\alpha}^4 - \Omega_{\alpha}^2 \left[ i \frac{\mathbf{F}_{\alpha}^{(0)} \cdot \mathbf{k}}{m_{\alpha}} + c_{s\alpha}^2 k^2 + \omega_{p\alpha}^2 + \omega_{c\alpha}^2 \right] - \frac{\Omega_{\alpha} \omega_{c\alpha}}{m_{\alpha}} \left( \mathbf{F}_{\alpha}^{(0)} \times \mathbf{k} \right) \cdot \mathbf{e}_B \right. \\ \left. + \omega_{c\alpha}^2 (\mathbf{k} \cdot \mathbf{e}_B) \left[ i \frac{\mathbf{F}_{\alpha}^{(0)} \cdot \mathbf{e}_B}{m_{\alpha}} + (c_{s\alpha}^2 k^2 + \omega_{p\alpha}^2) \frac{\mathbf{k} \cdot \mathbf{e}_B}{k^2} \right] \right\} - \prod_{\alpha=1}^2 \frac{\omega_{p\alpha}^2}{k^2} \left[ \Omega_{\alpha}^2 k^2 - \omega_{c\alpha}^2 (\mathbf{e}_B \cdot \mathbf{k})^2 \right] = 0, \quad (1)$$

where  $\Omega_{\alpha} = \omega - \mathbf{k} \cdot \mathbf{u}_{\alpha}^{(0)}$  is the Doppler shifted frequency,  $\omega_{c\alpha}$  is the cyclotron frequency,  $\omega_{p\alpha}$  is the plasma frequency,  $\mathbf{F}_{\alpha}^{(0)}$  is the Lorentz force,  $\mathbf{e}_B$  is the unit vector in the direction of the magnetic field and  $c_{s\alpha}$  is the sound velocity. Index  $\alpha$  denotes the corresponding media (jet or background).

In the previous work of Bohata et al. (2012), the numerical solution for the case of two identical plasma beams with the same velocities, but opposite directions, was found for various input parameters. The situation of the plasma jet interaction with the plasma background was studied as well and the numerical solution for this problem was found by Horký (2012, 2013).

The maximum of the imaginary part of the solution is denoted as the Plasma Instability Growth Rate (PIGR). This paper is focused on finding the plasma parameters for which this maximum occurs (the non-relativistic case and the plasma jet interaction with the plasma background are assumed). The calculations are performed on a microscopic level using the linear approximation. For the plasma parameters leading to the maximum of the imaginary part of the dispersion relation, the instability arises and amplitudes of all variables grow exponentially. In such a situation, the linear approximation is no longer valid, and other methods for modeling of the physical phenomena must be introduced. One of the possibilities is the Particle in Cell (PIC) simulation (e.g. Stockem et al. 2008). The results of these calculations can therefore be applied to: 1) The search for the instability regimes in which strong thermalization, turbulence, micro-reconnections on ion radius, non-thermal radiation, shock onset and other interesting phenomena can occur. The subsequent PIC simulations of the plasma behavior leading to significant phenomena seem to be the most reasonable next step for research in this regime. 2) The tests for the acceptance of the PIC codes (the PIC code must lead to an onset of instability for the parameters calculated by the method proposed in the next paragraph). Section 2 gives a short description of the algorithm used for calculation of complex roots of the GBDR relation. Section 3 discusses PIGR value dependences on various input parameters and geometrical situations.

## 2 METHOD

The following indices were designated in our analysis: “j” for parameters of the jet and “b” for parameters of the background. It is beneficial to transform the variables and the whole GBDR relation to a dimensionless form. After this step the relation is simply scalable and the equations are covariant in this transformation, which implies that the results can be used for both space and laboratory plasmas, such as thermalization in astrophysical jets or in fusion experiments. The relations for the dimensionless form were chosen with regard to the zero background velocity as in Horký (2012, 2013):

$$\bar{c}_{sj} \equiv \frac{c_{sj}}{u_j}, \quad \bar{c}_{sb} \equiv \frac{c_{sb}}{u_j}, \quad \bar{\omega}_{cj} \equiv \frac{\omega_{cj}}{\omega_{pb}}, \quad \bar{\omega}_{cb} \equiv \frac{\omega_{cb}}{\omega_{pb}}, \quad \bar{\omega}_{pj} \equiv \frac{\omega_{pj}}{\omega_{pb}}, \\ \bar{\omega}_{pb} \equiv \frac{\omega_{pb}}{\omega_{pb}} = 1, \quad \bar{u}_b \equiv \frac{u_b}{u_j}, \quad \bar{u}_j \equiv \frac{u_j}{u_j} = 1, \quad \bar{k} \equiv \frac{k u_j}{\omega_{pb}}, \quad \bar{\omega} \equiv \frac{\omega}{\omega_{pb}}, \\ \bar{\Omega}_j = \bar{\omega} - \bar{k} \cos \varphi \sin \theta_k, \quad \bar{\Omega}_b = \bar{\omega} - \bar{k} \bar{u}_b \cos \varphi \sin \theta_k. \quad (2)$$

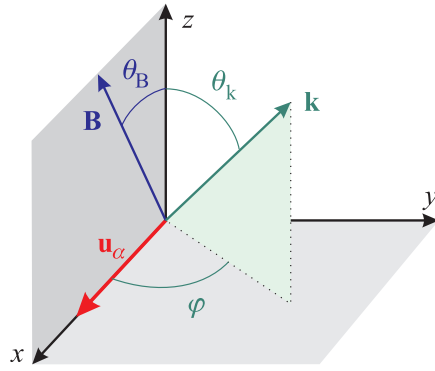


**Fig. 1** The system of coordinates used in calculations.

The reference system was set according to Figure 1, in which the directions of the respective vectors  $\mathbf{u}_\alpha$ ,  $\mathbf{B}$  and  $\mathbf{k}$  are drawn. The wave vector can point in any direction, the magnetic field vector lies in the  $(x-z)$  plane and the jet is directed along the  $x$ -axis. The vector coordinates are

$$\begin{aligned} \mathbf{u}_\alpha &= (u_\alpha, 0, 0), \\ \mathbf{B} &= (B \sin \theta_B, 0, B \cos \theta_B), \\ \mathbf{k} &= (k \cos \varphi \sin \theta_k, k \sin \varphi \sin \theta_k, k \cos \theta_k). \end{aligned} \quad (3)$$

After simple manipulation, the dimensionless form of the dispersion relation becomes (Horký 2012, 2013)

$$\begin{aligned} & \left[ \overline{\Omega}_j^4 + i \overline{\Omega}_j^2 \overline{\omega}_{cj} \overline{k} (G_1) - \overline{\Omega}_j^2 (\overline{c}_{sj}^2 \overline{k}^2 + \overline{\omega}_{pj}^2) - \overline{\Omega}_j^2 \overline{\omega}_{cj}^2 \right. \\ & \quad \left. - \overline{\Omega}_j \overline{\omega}_{cj}^2 \overline{k} (G_3) + (\overline{\omega}_{cj}^2 \overline{k}^2 \overline{c}_{sj}^2 + \overline{\omega}_{cj}^2 \overline{\omega}_{pj}^2) (G_2)^2 \right] \\ & \cdot \left[ \overline{\Omega}_b^4 + i \overline{\Omega}_b^2 \overline{\omega}_{cb} \overline{k} \overline{u}_b (G_1) - \overline{\Omega}_b^2 (\overline{c}_{sb}^2 \overline{k}^2 + 1) - \overline{\Omega}_b^2 \overline{\omega}_{cb}^2 \right. \\ & \quad \left. - \overline{\Omega}_b \overline{\omega}_{cb}^2 \overline{k} \overline{u}_b (G_3) + (\overline{\omega}_{cb}^2 \overline{k}^2 \overline{c}_{sb}^2 + \overline{\omega}_{cb}^2) (G_2)^2 \right] \\ & - \left[ \overline{\omega}_{pj}^2 (\overline{\Omega}_j^2 - \overline{\omega}_{cj}^2 (G_2)^2) \right] \cdot \left[ \overline{\Omega}_b^2 - \overline{\omega}_{cb}^2 (G_2)^2 \right] = 0, \end{aligned} \quad (4)$$

where the geometrical terms are denoted as

$$\begin{aligned} G_1 &= (\cos \theta_B \sin \varphi \sin \theta_k), \\ G_2 &= (\cos \varphi \sin \theta_k \sin \theta_B + \cos \theta_k \cos \theta_B), \\ G_3 &= (\cos^2 \theta_B \cos \varphi \sin \theta_k - \cos \theta_B \cos \theta_k \sin \theta_B). \end{aligned} \quad (5)$$

This dimensionless relation is a polynomial equation with complex roots of the 8<sup>th</sup> order. The algorithm developed by Hubbard, Shleicher and Sutherland (Hubbard et al. 2001) was used to find the solution. The algorithm was implemented in the Wolfram commercial software package Mathematica 8.0.1. Unlike the Newton-Raphson method, this algorithm can select seed values that later converge to solutions. The results are arranged into plots in which the real branches of the solution have a different style than the imaginary branches, and the maximum imaginary value that determines the PIGR value is highlighted. An example of the program's output is shown in Figure 2.

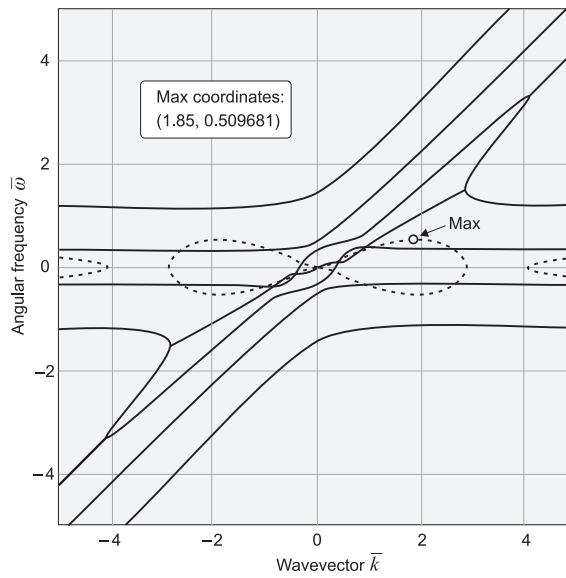


**Fig. 2** Real (*solid*) and imaginary (*dashed*) branches of the GBDR dispersion relation and PIGR value (denoted as Max) for  $\bar{\omega}_{cj} = \bar{\omega}_{cb} = 0.5$ ,  $\bar{c}_{sj} = \bar{c}_{sb} = 0.1$ ,  $\bar{\omega}_{pj} = 1$ ,  $\theta_k = \pi/2$ ,  $\varphi = 0$  and  $\theta_B = \pi/4$ . These values were used as initial values for the calculations, see Table 1 for details.

In the next step, the dependence of the PIGR value on various parameters of the dimensionless GBDR (such as cyclotron frequencies of the jet and the background, the sound velocities of the jet and the background, the plasma frequency of the jet and the directions of the magnetic field and of the wave vector) is found.

### 3 RESULTS

The PIGR value was calculated during the program cycle running from the minimum to the maximum value of the tracked parameter while other parameters were fixed at their initial values. Intervals of these parameters are shown in Table 1. It was not necessary to change the jet velocity, because its dimensionless value was fixed at 1.

**Table 1** Parameters used for the numerical solution. The dispersion relation for the initial values is depicted in Fig. 1.

Parameter	Initial value	Minimum value	Maximum value
$\bar{\omega}_{cj}, \bar{\omega}_{cb}$	0.5	0.1	3.0
$\bar{c}_{sj}, \bar{c}_{sb}$	0.1	0.1	1.5
$\bar{\omega}_{pj}$	1	1	5
$\theta_k$	$\pi/2$	0	$\pi/2$
$\varphi$	0	0	$\pi/2$
$\theta_B$	$\pi/4$	0	$\pi/2$

#### 3.1 The Dependence of the PIGR Value on the Cyclotron Frequencies

The cyclotron frequency of the jet and the cyclotron frequency of the background were increased from the minimum value of 0.1 to the final value of 3.0 with a step size of 0.1. The cyclotron

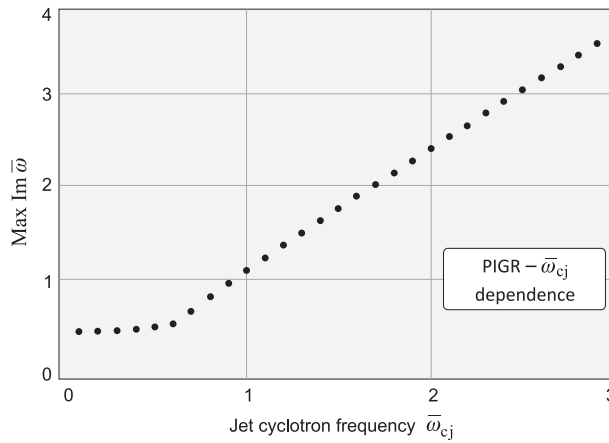


**Fig. 3** The dependence of the PIGR value on the jet cyclotron frequency.

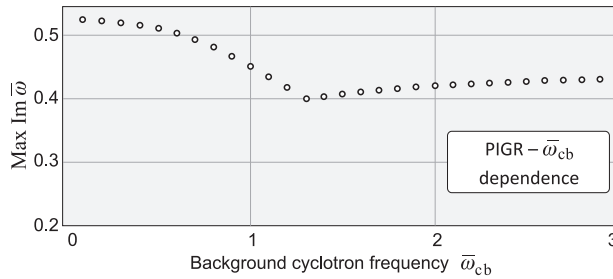


**Fig. 4** The dependence of the PIGR value on the background cyclotron frequency.

frequency is proportional to the magnetic field intensity influencing the charged particles. The dependence of the PIGR value on the cyclotron frequency of the jet is depicted in Figure 3, where the almost linear increase of this relation for  $\bar{\omega}_{cj} > 0.6$  is noticeable. The change of the slope at this point ( $\bar{\omega}_{cj} = 0.6$ ) corresponds to the location of the minimum for the two different imaginary branches of the dispersion relation. The dependence of the PIGR value on the cyclotron frequency of the background is more complicated than the case of jet cyclotron frequency. In Figure 4, the decrease of lower frequency values is visible. The curve reaches a minimum and then it rises to an asymptote. The minimum is numerically determined to be  $\bar{\omega}_{cb} = 1.313$  and the corresponding PIGR value is equal to 0.39795. This effect is caused by the fact that the solution has two imaginary branches in this area and while the value of  $\bar{\omega}_{cb}$  is increasing, the first branch is descending and the second is rising. At the minimum both branches have equal PIGR values.

### 3.2 The Dependence of PIGR Value on the Sound Velocities

Sound velocity is proportional to  $(T_\alpha/m_\alpha)^{1/2}$ , where  $T_\alpha$  is the plasma temperature, and  $m_\alpha$  is the mass of the jet or of the background particles (electrons or ions). The index  $\alpha$  labels the corresponding media (jet or background). Modification of the original Buneman dispersion relation by addition of the sound velocities of both media is a result of the calculation with non-zero pressure gradient, i.e. without the cold limit. The dimensionless parameter  $\bar{v}_s$  involves the plasma jet velocity, see

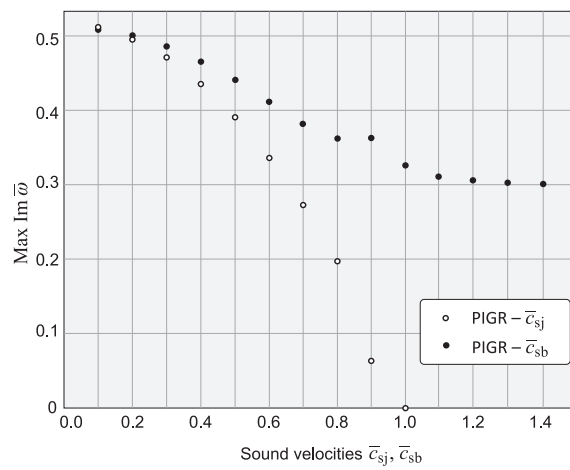


**Fig. 5** The dependence of the PIGR value on the sound velocities.

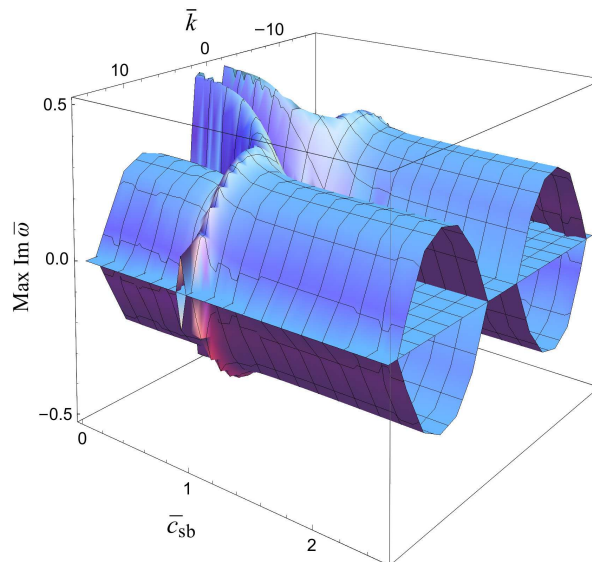


**Fig. 6** The dependence of the imaginary branches on  $\bar{c}_{sb}$ .

Equation (2), and  $\bar{c}_{sj} > 1$  indicates a subsonic jet while  $\bar{c}_{sj} < 1$  denotes a supersonic one. Both the sound velocity of the jet and the sound velocity of the background were increased from the initial value 0.1 to the final value 1.5 with a step size of 0.1. The dependence of the PIGR value on the sound velocities of both jet and background is depicted in Figure 5. The jet dependence (unfilled circles) shows a decreasing trend and the PIGR value is zero, while  $\bar{c}_{sj} \geq 1$ . This implies that for a subsonic jet (in dimensionless form the sound velocity equals 1) the GBDR relation has no imaginary branch and therefore the PIGR value is zero and no instabilities occur. The dependence of the PIGR value on the sound velocity of the background (filled circles) is more complicated. An interesting peak is located at the value  $\bar{c}_{sb} \doteq 0.9$ . We made a three-dimensional plot of the imaginary

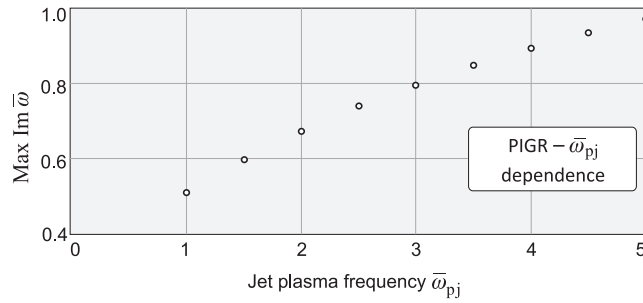


**Fig. 7** The dependence of the PIGR value on  $\bar{\omega}_{pj}$ .

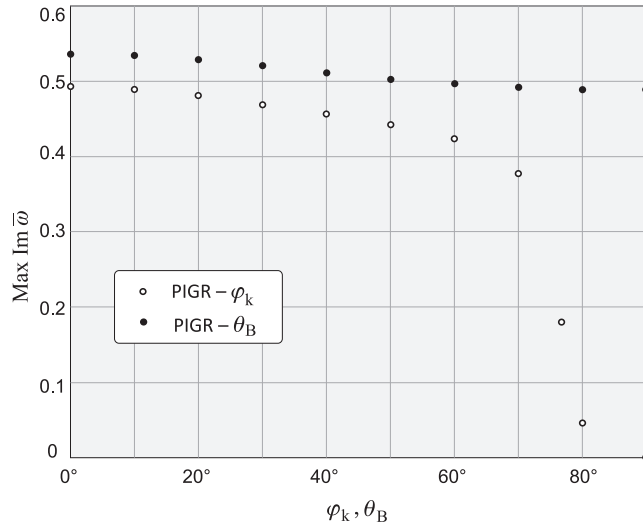


**Fig. 8** The dependence of the PIGR value on the magnetic field direction (*filled circles*) and on the wave vector direction (*unfilled circles*).

branches of the GBDR solution to uncover the origin of this local maximum. The result can be seen in Figure 6. The first axis corresponds to  $\bar{\omega}_{sb}$ , the second to  $\bar{k}$ , and the vertical axis to the value of the imaginary branch of the PIGR coefficient. This clearly shows that the peak originates from the ridge present in the solution of the dispersion relation.

### 3.3 The Dependence of the PIGR Value on the Plasma Frequency of the Jet

All dimensionless frequencies in the system are related to the background plasma frequency, see Equation (2). This means that the dimensionless plasma frequency of the background  $\bar{\omega}_{pb}$  is always equal to 1, see Equation (2). The dimensionless plasma frequency of the jet  $\bar{\omega}_{pj}$  is in fact the ratio of the jet to the background plasma frequencies. This parameter is therefore proportional to  $(n_{ej}/n_{eb})^{1/2}$ . During the numerical calculation it was increased from the initial value 1 to the final value 5 with a step size of 0.5. It is a rather big step, but as can be seen in Figure 7, the dependence is very simple and does not have any discontinuities or local maxima or minima.

### 3.4 The Dependencies of the Directional PIGR Value

The dependence of the PIGR value on the magnetic field direction is simply predictable from the Lorentz equation of motion. A longitudinal magnetic field will evoke less disturbances than a perpendicular one. As can be seen in Figure 8, the PIGR value has a maximum at  $\theta_B = 0$  (perpendicular direction) and decreases for increasing  $\theta_B$ . The dependence of PIGR value on the direction of the wave vector is also predictable due to the dot product between  $\mathbf{k}$  and  $\mathbf{u}_\alpha$  in the GBDR relation, so if the angle between the wave vector and the velocity equals  $90^\circ$ , the PIGR value should be zero.

In Figure 8, the dependence shows a decreasing trend and it is zero at the angle  $90^\circ$ . Because of the cylindrical symmetry, both angles  $\varphi_k$  and  $\theta_B$  were only varied from  $0^\circ$  to  $90^\circ$  with a step size of  $10^\circ$ .

## 4 CONCLUSIONS

Plasma jets from black holes and other types of astronomical objects are driven by magnetic fields, and classical Buneman instability analysis (without magnetic fields) is inapplicable. All calculations must be performed using the GBDR with nonzero pressure gradient and nonzero magnetic fields. The PIGR as the maximum of the imaginary parts of the GBDR relation was numerically calculated in this paper. The PIGR value is responsible for a strong thermalization during the jet-background interaction and these calculations can be useful for understanding the underlying processes. Furthermore, the known PIGR value can be used as a simple test of PIC numerical methods frequently used for plasma jet simulations. It is an interesting but still an open question as to whether the PIGR value could be analytically directly calculated from the dimensionless GBDR relation. The dispersion relation is not anisotropic in velocity space. This possibility can cause other phenomena, e.g. particle acceleration, shock origin, etc. (Nishikawa et al. 2005; Mizuno et al. 2009, and references therein), which will be the topic of detailed PIC simulations.

**Acknowledgements** Research described in this paper was supported by the Czech Technical University in Prague with grants SGS10/266/OHK3/3T/13 (Electric discharges, basic research and application), SGS12/181/OHK3/3T/13 (Plasma instabilities and plasma-particle interactions) and by the Grant Agency of the Czech Republic with grant GD205/09/H033 (General relativity and its applications in astrophysics and cosmology).

## References

- Bohata, M., Břen, D., & Kulhánek, P. 2012, ISRN Condensed Matter Physics, 2011, 896321
- Bonanno, A., & Urpin, V. 2011, A&A, 525, A100
- Buneman, O. 1959, Physical Review, 115, 503
- Horký, M. 2012, Numerical Solution of the Generalized Buneman Dispersion Relation, Proceedings of Poster 2012, Prague, 2012
- Horký, M. 2013, Instability Growth Rate Dependence on Input Parameters During the Beam–Target Plasma Interaction, Acta Polytechnica 53(2), 174
- Hubbard, J., Schleicher, D., & Sutherland, S. 2001, Inventiones Mathematicae, 146, 1
- Mizuno, Y., Zhang, B., Giacomazzo, B., et al. 2009, ApJ, 690, L47
- Murphy, G. C., Lery, T., O’Sullivan, S., et al. 2008, A&A, 478, 453
- Nishikawa, K.-I., Hardee, P., Richardson, G., et al. 2005, ApJ, 622, 927
- Silk, J., Antonuccio-Delogu, V., Dubois, Y., et al. 2012, A&A, 545, L11
- Stockem, A., Dieckmann, M. E., & Schlickeiser, R. 2008, Plasma Physics and Controlled Fusion, 50, 025002
- Urpin, V. 2006, A&A, 455, 779